Vinogradov V, Knyazhansky M, Tsun A.

Effects of local overloads on cold rolling mill work rolls.

***International Journal of Mechanical Sciences* 2017, 123, 106-116**

Effects of local overloads on cold rolling mill work rolls

V. Vinogradov [a1], M. Knyazhansky [b], A. Tsun[c]

[a] School of Civil Engineering and Geosiences, Newcastle University, Newcastle upon Tyne, NE1 7RU, U.K.

[b] Department of Software Engineering, Shamoon College of Engineering, Beer-Sheva, 84100, Israel

[c] Raymond and Beverly Sackler Faculty of Exact Sciences, School of Physics and Astronomy, Tel-Aviv University, Tel-Aviv, 69978, Israel

Abstract

Local overloading is one of the most common reasons for premature failures of cold rolling mill work rolls. Case-hardened rolls demonstrate spatial variation of the material hardness and yield strength with a decreasing profile with depth and belong to the class of so-called plastically graded materials. Contact overloads cause formation of subsurface closed-shape plastic zones, accompanied by a significant perturbation in the stress field. In the present paper the effect of an overload on a case-hardened roll is numerically modelled using finite element, when the parameters of the contact loads are chosen to represent a common situation when an accidentally formed strip fold enters the roll bite. It is shown that plastic deformations in the graded layer originate at depths, which significantly exceed the depth of the maximum effective stresses, determined by the elastic solution. During the contact overload, tensile stresses develop at the upper boundary between the elastic and plastic zones. Tensile stresses at the free surface in the vicinity of the contact zone increase up to ten times due to formation of the subsurface plastic zone. Residual stresses with a very large tensile hydrostatic component are shown to appear in the unloaded material. These tensile stresses, both operational and residual, can cause premature spalling in the contact surface during either the overloading or further operation of the roll. It is shown that an increase in the depth of the hardened case and increase in the roll core hardness allows to reduce plastic deformations during overloads, reduce both operational and residual stresses in the graded layer and shift formation of the plastic zone deeper from the surface and the contact zone, which decreases the chances of premature spalling.

Keywords: Case hardening, Plastically graded materials, Plastic zone, Hertzian contact, Contact overloading

[1] Corresponding author: Vladimir.Vinogradov@newcastle.ac.uk

1. Introduction

Work rolls of cold rolling mills experience high contact loadings during their life. A roll system and a draft schedule of the rolled strip are usually designed such that the stresses acting at the roll-strip contact zone and near-contact zones within the work rolls do not exceed 50-90% of the elastic limit (or the yield stress σ_Y) of the roll material [1, 2]. When the contact length of two contacting bodies significantly smaller than their size, the distribution of the effective stress as well as the maximum shear stress along the depth direction exhibits a maximum. In the simplest case of frictionless contact of two cylinders, the peak of the distribution is located on the axes of symmetry at depth 0.4-1.0 of half the contact length, depending on the contact pressure distribution, and at 0.785 of half the contact length in the classical Hertz contact problem when the contact pressure has an elliptical distribution along the contact. The maximum value of the distribution is mainly determined by the maximum value of the contact stresses, while the depth depends on the contact length. If frictional forces are present at the contact zone the distribution maximum is shifted closer to the surface [3]. In order to increase the contact strength of the rolls they undergo surface hardening (quenching), followed by tempering. Surface or case hardening to the designed depth mentioned above increases the hardness and the yield stress of the surface layers and leads to the situation when the maximum effective stress is below the *local* elastic limit of the roll material. This ensures long-term life of the strengthened rolls without the inception of plastic deformations and irreversible damage in the designed working regimes. The profile of the yield strength with depth is hence non-uniform decreasing nonlinearly from the high strength at the near-contact surface to a lower in the core; the elastic properties of the material are practically remain unchanged. The roll material can then be considered as elastically homogeneous with a plastically graded surface layer.

The situation changes significantly when in some areas of the contact region the operating stress exceeds the local elastic limit and the material transfers into the elastic-plastic state. This not rarely happens in practice due to accidental overloads [4-6]. A very common issue in the steel industry is when the rolled strip folds ("pinches") in the roll bite due to strip breakage or non-uniform deformation of the strip across its width (see e.g. [5-6]), which can occur for several technological reasons [7-9].

Figure 1 schematically shows the distribution of the yield strength along the depth of hardened zone σ_s (curve 1) and the values of the effective stress σ_i on the symmetry axis of the loading area (curve 2), corresponding to regular working conditions. During the passage of the strip folds through the roll gap,

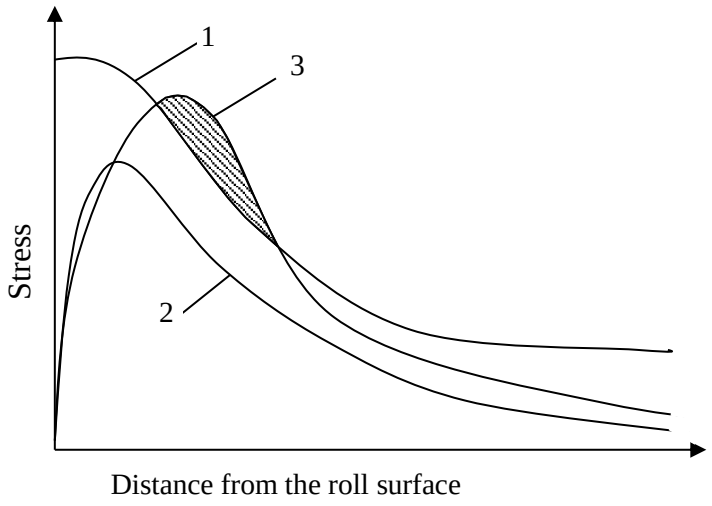

Figure 1. Inception of the plastic zone in the graded layer of the roll: 1 - distribution of the yield stress of the material; 2 - distribution of effective stresses under normal rolling conditions; 3 - distribution of the effective stress during passage of folds.

the contact stresses and hence the effective stress σ_i increase significantly (curve 3) and becomes greater than the yield strength (shaded area), which leads to a transition of the region into the plastic state. At this moment the original linear problem of loading of the elastic homogeneous body turns into a nonlinear problem of deformation of a plastically graded body, i.e. deformations of an elastic body with a pliant elastic-plastic inclusion with evolving boundaries influenced by the boundary conditions at the contact.

Practical research has established an unequivocal relationship between local overloads and subsequent damage (spalling, delamination, cracks) in the case-hardened rolls [7,9]. In the present paper numerical modelling of contact overloads is presented with particular attention to development of plastic deformation and both operating and residual stress perturbations in the case-hardened materials in an attempt to estimate the effects of overloads on further material durability.

2. Evaluation of force and geometrical parameters of local overloads

In this section an estimate is presented for the contact loads in the roll bite in normal operational conditions and in the incidental situation, when a triple fold passes through the roll bite. The exercise is for illustrative purposes only. The goal is to estimate the possible range of the normal contact loads and to demonstrate the potential of joint plastic deformation of the strip and the roll in the abnormal loading conditions.

Parameters of deformation during the passage of a triple strip thickness are estimated using the model suggested by Tselikov, see e.g. [7,8]. The actual length of the deformation zone is determined by the method of Hitchcock, described in e.g. [1,10-12], which takes into account the roll flattening effect. The results of calculations for a low-carbon steel are shown in Table 1. The diameter of the work rolls is taken $D = 500$ mm and for normal operation the relative reduction is 25%.

Our calculations indicate that the contact pressure in of triple thickness through the roll bite increases by 3 to 5 times, while the total loads increase even more intensively by up to 8 times, and the contact length increases by 3-4 times.

Due to the assumed incidental overloading the relative draft increases from 25% to about 70%. The coefficient of friction increases from ~0.1 to ~0.2 (and more) due to discontinuities in the lubricant layer between the roll and the strip (partially dry friction). The values for the coefficient of friction during cold rolling with and without lubrication are chosen from the data presented in Table 3.12 in [10]. Specific contact pressure increases significantly when the thickness of the strip approaches the limiting (minimum possible) thickness h_{min}, which is roughly determined by the relation [13,14]

$$h_{min} = 3.62\, f\, D\, K_1/E, \tag{1}$$

where E is the Young modulus of the material and K_1 is the constrained yield stress, for details see e.g. [1,12]. Therefore, the roll gap, set for normal operation regimes (for instance, 1mm), can become less than h_{min} due to the increased coefficient of friction (for $f = 0.2$ the limiting minimum thickness is already 1.034 mm, which is higher than the considered roll gap). The relation (1) is also shown graphically in Figure 2 for illustration. In these situation, a joint plastic deformation of both the strip and the rolls becomes possible.

Table 1. Parameters of the deformation zone of rolling strip folds

Parameters	Thickness of the rolled strip, mm	Rolling folds of triple thickness, ε_1= 70%				Rolling in the normal conditions, ε_1=25%.
		Constrained yield strength of the material in the deformation zone K_1				
		K_1=0.6 GPa		K_1=0.4 GPa		K_1=0.6 GPa
		friction coefficient f		friction coefficient f		friction coefficient f =0.1
		f =0.1	f =0.2	f =0.1	f =0.2	
Length of the deformation zone, mm	0.5 - 1	35-40	40 -45	28 -35	33 -38	12 - 15
	2 - 3	60 - 65	65 - 67	57 - 62	60 - 63	15 - 20
Mean pressure on the roll, GPa	0.5 - 1	1.2 - 1.7	2.5 - 3	0.75 - 0.9	1.8 - 2.2	0.8 - 1.3
	2 - 3	0.9 - 1.3	1.4 - 2.2	0.6 - 0.8	0.8 - 1.7	0.9 - 1.1
Total load on the roll per mm width, F_n, kN/mm	0.5 - 1	40 - 65	120 - 170	25 - 35	75 - 82	12 - 17
	2 – 3	60 - 70	70 - 150	38 - 42	55 - 110	16 - 22
Limiting thickness, $h_{\min}$,mm		0.52	1.035	0.3	0.66	

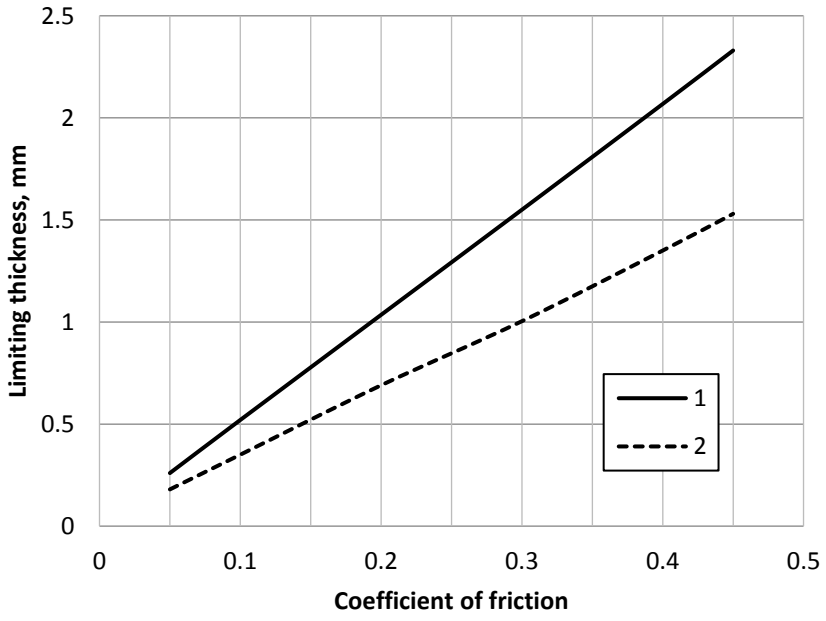

Figure 2. Limiting thickness h_{min} achievable in flat rolling as a function of average coefficient of friction for constrained yield stress of $K_1 = 0.6$ GPa (1) and $K_1 = 0.4$ GPa (2).

3. Problem formulation

Previous experiments and numerical modelling of local contact loading of cylinders with a plastically graded surface layer [15] have shown that plastic deformation initiates with formation of a closed-shape plastic region at some depth without reaching the surface. Maximum plastic strains form at the depths of $1.5-2$ of half the contact length b, which exceed the depth at which the maximum effective stress develops in purely elastic contact conditions ($0.785b$, according to the Hertz solution). Due to the spatial variation of the yield strength the plastic zones are shifted deeper towards the layers of lower values of the yield stress, while an extended narrow zone below the contact area remains elastic, behaving as an elastic beam on a ductile substrate.

In order to understand the inception and development of plastic deformation in a case-hardened roll due to passage of a fold through the roll bite, a simpler problem is formulated herein. We consider a two-dimensional problem of a case-hardened half-plane, representing the roll, with a plastically graded surface layer in contact with an elastic circular disc, while the total contact load and the radius of the disc are chosen such that the corresponding loading parameters (mean load pressure p and contact length $2b$) are in accordance with the estimates of the illustrative example, described in the previous section (Table 1). Validation of the model can be found in [15]. The straight boundary eliminates the influence of the contact surface curvature of the plastically graded body on the distribution of stress/strain fields in the near-contact zones. However, for contact lengths comparable with the depth of the hardened layer and radii of the work roll significantly greater than the contact zone length, this is seen as an acceptable approximation. Contact is treated as frictionless. The influence of contact friction, the shape of the distribution of contact stresses along the contact and the curvature of the contact surface will be discussed elsewhere.

The required radius R of the pressing disc was determined using the Hertz solution:

$$b = \sqrt{\frac{8F_n R}{\pi E_e}}, \tag{2}$$

where F_n is the force pushing the disc onto the half-plane (per unit thickness), and E_e is the combined Young's modulus, determined by the expression

$$E_e = \frac{2E_c E_p}{(E_c + E_p)(1-\nu^2)}. \tag{3}$$

The origin of coordinate system is placed in the middle of the contact area, the X-axis points horizontally to the right along the contact surface and the Y-axis upwards, being the axis of symmetry. Elliptic (Hertzian) pressure distribution along the contact is given by the relation

$$p = p_{max}\sqrt{1-\left(\frac{x}{b}\right)^2}, \tag{4}$$

where p_{max} denotes the maximum pressure at $x = 0$, determined as

$$p_{max} = \sqrt{\frac{F_n E_e}{2\pi R}}. \tag{5}$$

Hereinafter the contact conditions are set to represent the illustrative example of Table 1: for normal operation the contact zone length $2b$ is chosen from the range $12-20$ mm, and for a fold passing through the roll gap from the range $28-65$ mm. The contact force F_n is chosen from the range of $15-20$ kN/mm for normal operation, and from the range of $60-150$ kN/mm for the case of overloading.

The required radius of the pressing disk is determined based on the considered loading parameters, for instance, for $F_n = 60$ kN/mm with $2b = 35$ mm and $2b = 65$ mm, the disk radius corresponding to the perfectly elastic contact, should be $R = 350$ mm and $R = 1355$ mm, respectively. In order to maintain the magnitudes of the contact force and length with developed plastic deformation (nonlinear elastic-plastic problem), the disk radius is then iteratively adjusted by simulating the elastic-plastic contact problem and amending R until the contact length reduces to the required value.

Three cases of the roll material hardness and yield stress distribution with the depth of the graded surface layer are analyzed (Figure 3): 1 – total depth of the hardened layer is 72 mm and a softer core; 2 – total depth of the hardened layer is 46 mm and a softer core; 3 – total depth of the hardened layer is 46 mm and a harder core. Case 2 is taken as a basis for analysis of the effects of increase in the thickness of the hardened layer (Case 1) and increase in the core yield strength (Case 3).

Based on accurate experimental measures of micro-hardness distribution in a surface-quenched tool steel [15] (with 0.9% C, 2% Cr) , the yield strength distribution $\sigma_{sy}(y)$ with depth (along the Y axis) is assumed to be most accurately described by the following Weibull-type exponential function:

$$\sigma_{sy} = \sigma_{s0}\left(c + de^{-ay^n}\right), \tag{6}$$

where σ_{s0} denotes the maximum value of the yield strength at $y = 0$, y is measured here along the negative direction of the Y-axis. The parameters of distribution (6) are chosen based on existing literature data on hardness distribution in case-hardened rolls (see, e.g. [1,7,8]). For a heat-treated hardened chromium steel (e.g. 0.9% C, 2% Cr, 0.15% V, 0.25% Mo) with a hardness of about 8.5–9 GPa the accepted value of the offset yield strength is $\sigma_{s0} = \sigma_{0.2} = 1.8$ GPa.

Factors in equation (6):

a is the scale parameter, which controls the length of the hardened zone, $a = 0.01$ for curve 1 in Figure 3 and $a = 0.04$ for curves 2 and 3, when y is measured in cm;

n is the shape parameter, which controls the length of the degreasing interval, $n = 3$;

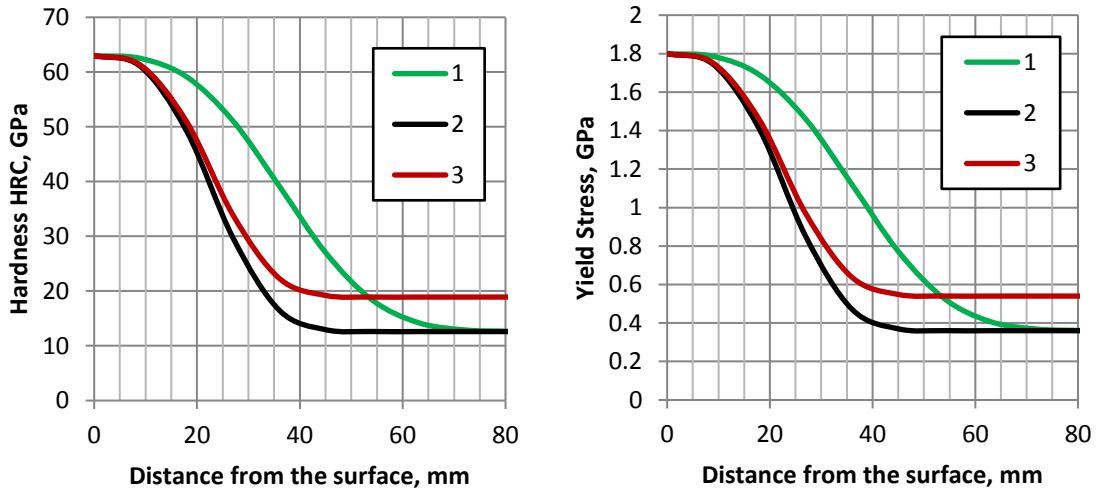

Figure 3. Distributions of hardness (left) and yield stress (right) with depth in the case-hardened roll used in simulations: 1 – total depth of the hardened layer is 72 mm and a softer core (green); 2 – total depth of the hardened layer is 46 mm and a softer core (black); 3 – total depth of the hardened layer is 46 mm and a harder core (red). This color scheme is maintained throughout the paper.

c and d $(c + d = 1)$ are coefficients, which define the ratio of the yield stresses of the surface and the core of the roll, $c = 0.2$, $d = 0.8$ for curves 1 and 2 in Figure 3 and $c = 0.3$, $d = 0.7$ for curve 3.

In order to analyze the effect of the subsurface plastic zones on the near-contact stress field, the numerical solution of the contact problem for a plastically graded half-plane is compared to the solution of the contact problem for a half-plane in which the yield strength of the material are assumed constant at 1.8 GPa, same as the value at the surface of the plastically graded half-plane. This is to demonstrate the difference between of the stress and strain field of the case-hardened material with the subsurface elastic–plastic zone and the design model when the material is assumed homogeneous elastic. The loading disc is assumed to be perfectly elastic in all the simulations. Behavior of the half-plane material beyond the elastic limit is approximated by adopting linear strain hardening. The average value of the hardening modulus at strains of 0–10% is accepted at 3 GPa, based on systematic experimental mapping of micro-hardness increments due to plastic deformation presented in [15].

Numerical modelling of deformation of the plastically graded material in contact is carried out by the finite element method using commercial software 'Comsol-4' [16]. Due to symmetry with respect to the vertical axis, calculations are performed for the right half of the model. The size of the truncated domain of the modelled half-plane was chosen under the following considerations. For the solution of the elastic contact problem of a loaded half-plane of infinite size the zone with significant values of strains and stresses (more than 15-20% of their maximum values) for the contact length of 35 mm and 65 mm lays inside the rectangle ($x = 150$ mm, $y = -200$ mm), when the values of the strain and stress of more than 50% of the maximum values of these parameters are obtained in the contact zone with the dimensions of ($x = 60$ mm, $y = -100$ mm). In order to minimize the influence of the size of a half-plane on the results, the size of the modeled half-plane was chosen 10 times larger than the rectangle with significant values, i.e. ($x = 1500$ mm, $y = -2000$ mm). The half-plane FE model was constructed in the form of a grid with variable mesh size and was divided into 3 regions (Figure 4). The size of contact region area, where the expected value of the strain and stress were more than 50% of the

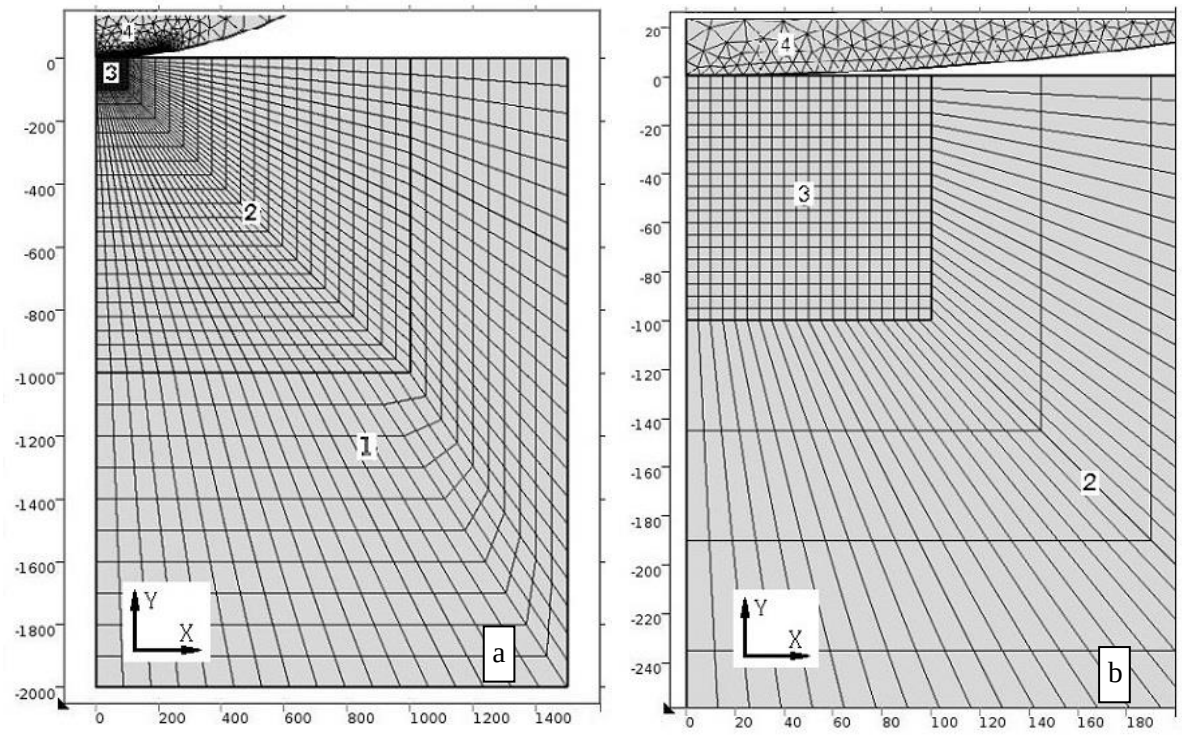

Figure 4. Finite element mesh for the solution of the contact problem. (a) – general view of the mesh; (b) – enlarged view of the contact region of the grid.

maximum values of these parameters with maximum gradients of change, was chosen as 100×100 mm (zone 3 in Figure 4) and was meshed with a grid of square elements of length 5 mm, i.e. each side of the square was divided into 20 elements. The intermediate region 2 with the increased length of the elements was located between the coordinates ($x = [100, 1000]$ mm, $y = [-100, -1000]$ mm). Each side of the obtained polygon was divided into 20 elements, and the grid is formed as shown in Figure 4. The peripheral region 3 ($x = [1000,1500]$ mm, $y = [-1000, -2000]$ mm) is approximated by a grid with large step, as shown in Figure 4. Zone 4 is the loading disk with a mesh of triangular elements.

Zero-displacement boundary conditions were applied to the bottom surface of the domain. Traction-free boundary conditions were applied to the lateral face and the part of the upper surface not in contact with the loading disk. Symmetry conditions were applied along the axis *Y*. Force *F* was applied to the disk along the negative direction of the axis *Y*. The radius of the disk was iteratively updated as described above in order to maintain the magnitude of the total contact force and the contact length as prescribed parameters for analysis and comparison of their effects. Unloading was performed by removal the force *F*, acting on the disc, for evaluation of residual stresses caused by plastic deformation in the half-plane.

Inception, shape and parameters of the plastic zone are determined by the values of the second invariant of the plastic strains, which defines the effective plastic strain ε_e^p. As usual, plastic strains ε_{ij}^p are determined as the difference between total strains ε_{ij} and elastic strains ε_{ij}^e.

4. Numerical results

4.1 Plastic strain distribution

Inception of plastic zones in plastically graded half plane is observed both for the contact length of $2b = 35$ mm and $2b = 65$ mm when loaded with forces greater than $F_n = 60$ kN/mm. Figure 5 shows an example of the effective plastic strain distribution with $2b = 35$ mm and $F_n = 60$ kN/mm. Due to non-uniform distribution of the yield stress with depth, the plastic zone is shifted with respect to the location of the maximum effective stress σ_e deeper into the core with a lower yield stress. Above the

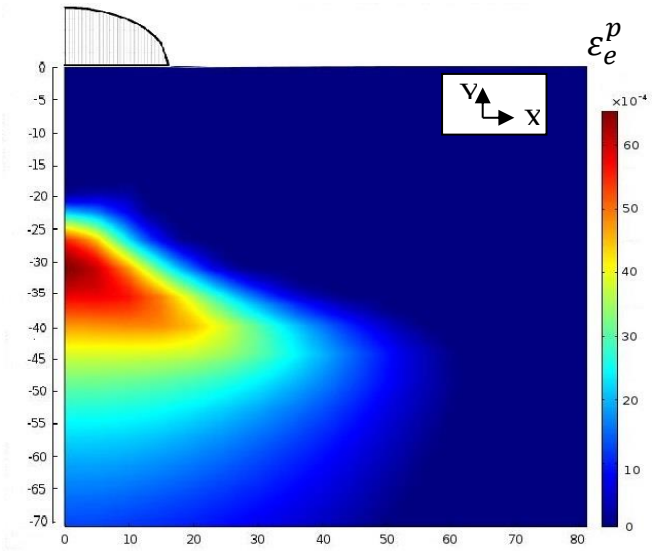

Figure 5. Inception of a plastic zone in the graded layer of 46 mm depth (curve 2 in Figure 3) with the contact length of 35 mm and load $F_n = 60$ kN/mm. Distribution of contact pressure is shown schematically to indicate the contact length. Color map represents the level of effective plastic strain, dark blue field – zone of zero plastic strain. X and Y coordinates are in mm.

plastic zone a shallow wide area forms, which remains elastic. In fact, it acts as an elastic beam on a ductile substrate and the stress field in the half-plane changes significantly.

Plastic strains reach their maximum values along the axis of symmetry Y ($x = 0$). Figure 6 shows distributions of the effective plastic strain along the Y axis for different parameters of the hardened layer and contact loads. Explanation of different parameter values corresponding to curves 1-10 in Figure 6a-6d is given in Table 2.

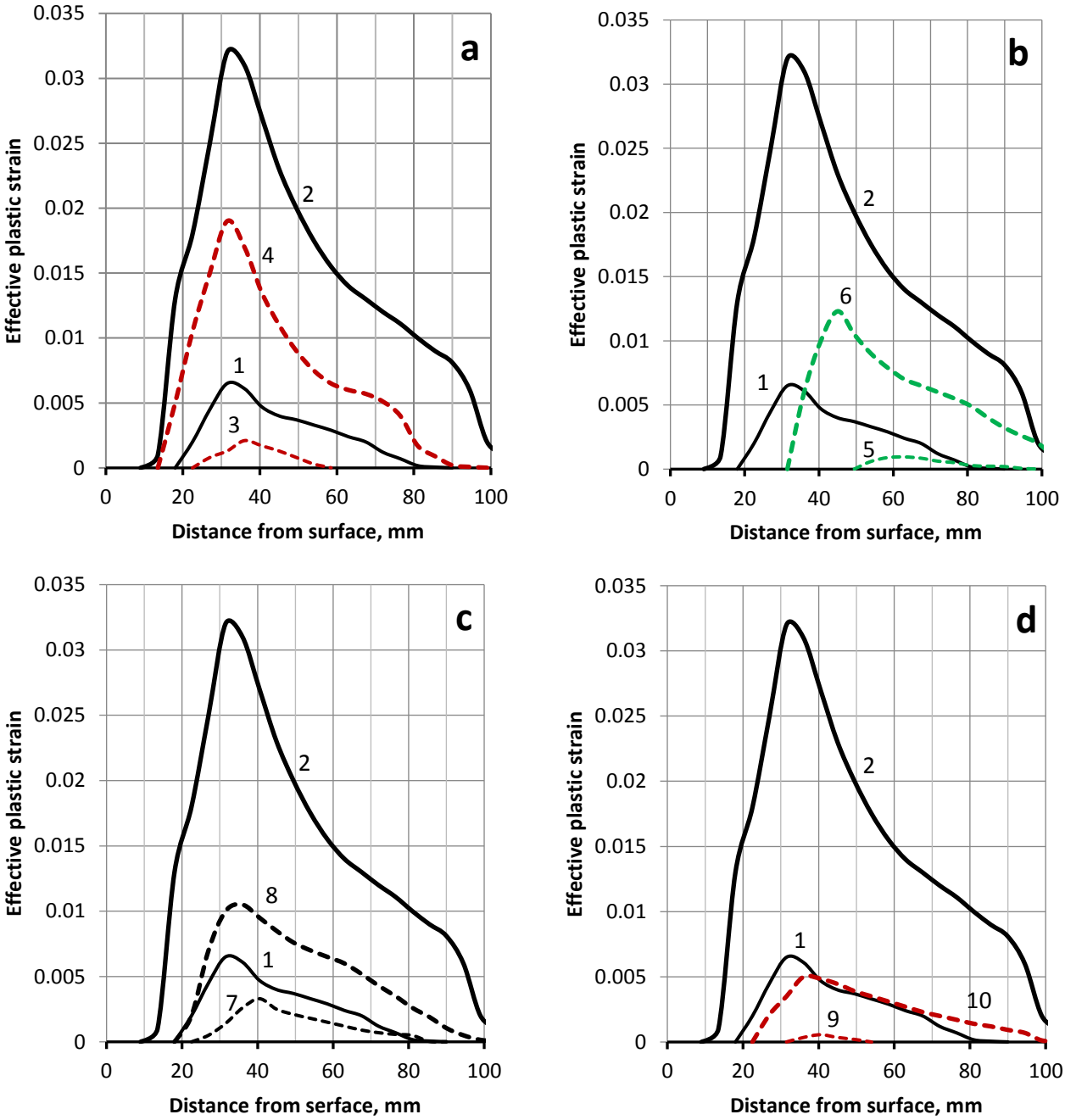

Figure 6. Distribution of the effective plastic strain along the axis of symmetry Y at different parameters of the graded surface layer and contact loads: (a) – effect of the core yield strength, ratio σ_{sy}/σ_{s0}; (b) – effect of the total depth of the hardened zone H_z; (c) – effect of the contact zone length $2b$; (d) – joint effect of the contact length $2b$ and core yield strength. Parameters corresponding to different curves are shown in Table 2.

Table 2. Parameters of the graded (hardened) surface layer and of the surface load (characteristic of the curves in Figure 6)

Curve no. Figure 6	Total depth of hardened zone H_z, mm	Contact length $2b$, mm	Yield strength of the core material, σ_{sv}/σ_{s0}	Total pressure on the contact per 1 mm width F_n, kN/mm
1	46	35	0.2	60
2	46	35	0.2	100
3	46	35	0.3	60
4	46	35	0.3	100
5	72	35	0.2	60
6	72	35	0.2	100
7	46	65	0.2	60
8	46	65	0.2	100
9	46	65	0.3	60
10	46	65	0.3	100

Comparison of the basic realization (curves 1 and 2) with other combinations of hardened surface and loadings indicates that:

As it might be expected, increase in thickness of the hardened layer, all other factors being equal, leads to a decrease of the plastic strains in the zone of local overloading, and to shifting of the plastic zone deeper into the core (curves 5 and 6 in Figure 6b).

Increase in the core hardness with the same thickness of the hardened layer as in the base one (Figure 6a, curves 3 and 4) allows to reduce the magnitude of the plastic strains, but to a lesser extent than in the previous case of Figure 6b.

Figure 6c indicates a strong influence of the contact load magnitude on the development of plastic deformation in the hardened material in all the considered cases. Increasing the contact force by 1.6 times (from $F_n = 60$ kN/mm to $F_n = 100$ kN/m) leads to an increase of the effective plastic strain by up to 5-7 times. Similar effect is observed for the mean contact pressure. Decreasing of the mean contact pressure in about 2 times when the contact length increases from $2b = 35$ mm to $2b = 65$ mm, the maximum plastic strain decreases by a factor of 3.2 (Figure 6c, curves 7,8). Simultaneous change of the factors leads to their influence being amplified (e.g., Figure 6d, curves 9,10).

It is also interesting to analyze the inception of plastic deformation in the graded layer. Table 3 shows the results of simulations for different cases of loading of thin strips. The case of through-hardened roll, when the material remains in elastic zone, is also presented for comparison (Table 3, case D). Table 3 shows results for the base case (B), the case of thicker hardened surface layer (A) and the case with a core of an increased hardness (C).

Noteworthy is the fact that in each realization of the hardened case (A, B, C) initial plastic deformations (accepted at $\varepsilon_{ip} = 10^{-4}$ in our simulations) occur at closed values of the contact force F_n over the considered range of contact lengths $2b$. Herewith the depth of plastic zone inception h_{p0} significantly exceeds the depth of the maximum effective stress h_{sm}. As expected, in the through-hardened body (realisation D) plastic deformation occurs at the same depth as the maximum effective stress and under contact forces significantly larger than with graded surface layers (realization D1). In order for the plastic zone to form at the same depths as in cases A, B, C, both the contact length and the contact forth on the homogeneous material should be much larger (realization D2).

Table. 3. Inception of residual plastic strains in graded surface layers.

Parameters	Total depth of hardened zone $H_z = 72$ mm, softer core, $\sigma_{sv} = 0.38$ GPa $\sigma_{s0} = 1.8$ GPa		Total depth of hardened zone $H_z = 46$ mm, softer core, $\sigma_{sv} = 0.38$ GPa $\sigma_{s0} = 1.8$ GPa		Total depth of hardened zone $H_z = 46$ mm, harder core, $\sigma_{sv} = 0.57$ GPa $\sigma_{s0} = 1.8$ GPa		Through-hardened body $\sigma_{s0} = 1.8\ GPa$	
Realization	A		B		C		D	
	1	2	1	2	1	2	1	2
Contact length $2b$, mm	28	45	28	45	28	45	28	105
Contact force F_n, KN/mm corresponding to plastic strain $\varepsilon_{ip} = 10^{-4}$	52	54	34	34	47	55	80	285
Depth of plastic zone inception h_{p0}, mm	65	66	41	41	39	41	10.5	40
Depth of the maximum effective stresses h_{sm}, mm	10.5	17	10	16	10	16	10.5	39
Normalized depth of plastic zone inception, h_{p0}/b	4.64	2.93	2.93	1.82	2.78	1.82	0.75	0.76
Normalized depth of the maximum effective stresses h_{sm}/b	0.75	0.76	0.72	0.71	0.72	0.71	0.75	0.75
Mean normal contact pressure p_a, GPa	1.86	1.2	1.21	0.76	1.68	1,22	2.85	2.71

4.2 Operational and residual stresses

Inception of a plastic zone, when the material form residual plastic deformations, leads to perturbations in the operational stress fields in the near-contact surface layers, as well as development of local residual stresses in the vicinity of the plastic zone during unloading. With further operation of the roll, even in the designed working conditions, stresses acting in the region of previous local overloading superimpose on the residual stresses. Even if no failure occurs due to a single overloading, material deformation capacity decreases sharply in the zones of cumulative stresses and the probability of premature failure increases with subsequent operation of the rolls.

Figure 7 shows an example of operational stresses distribution (σ_{xa}, σ_{ya}) and residual stresses (σ_{xr}, σ_{yr}) due to loading of the elastic-plastic half-plane with the hardened case thickness of 46 mm (Figure 3, curve 2) when the contact length is $2b = 35$ mm and the contact force $F_n = 60$ kN/mm. One can see formation of an anomalous zone of tensile stresses $\sigma_{xa} > 0$ (Figure 7a). Tensile stresses $\sigma_{xa} > 0$ can also be observed at the free surface in the vicinity of the contact zone.

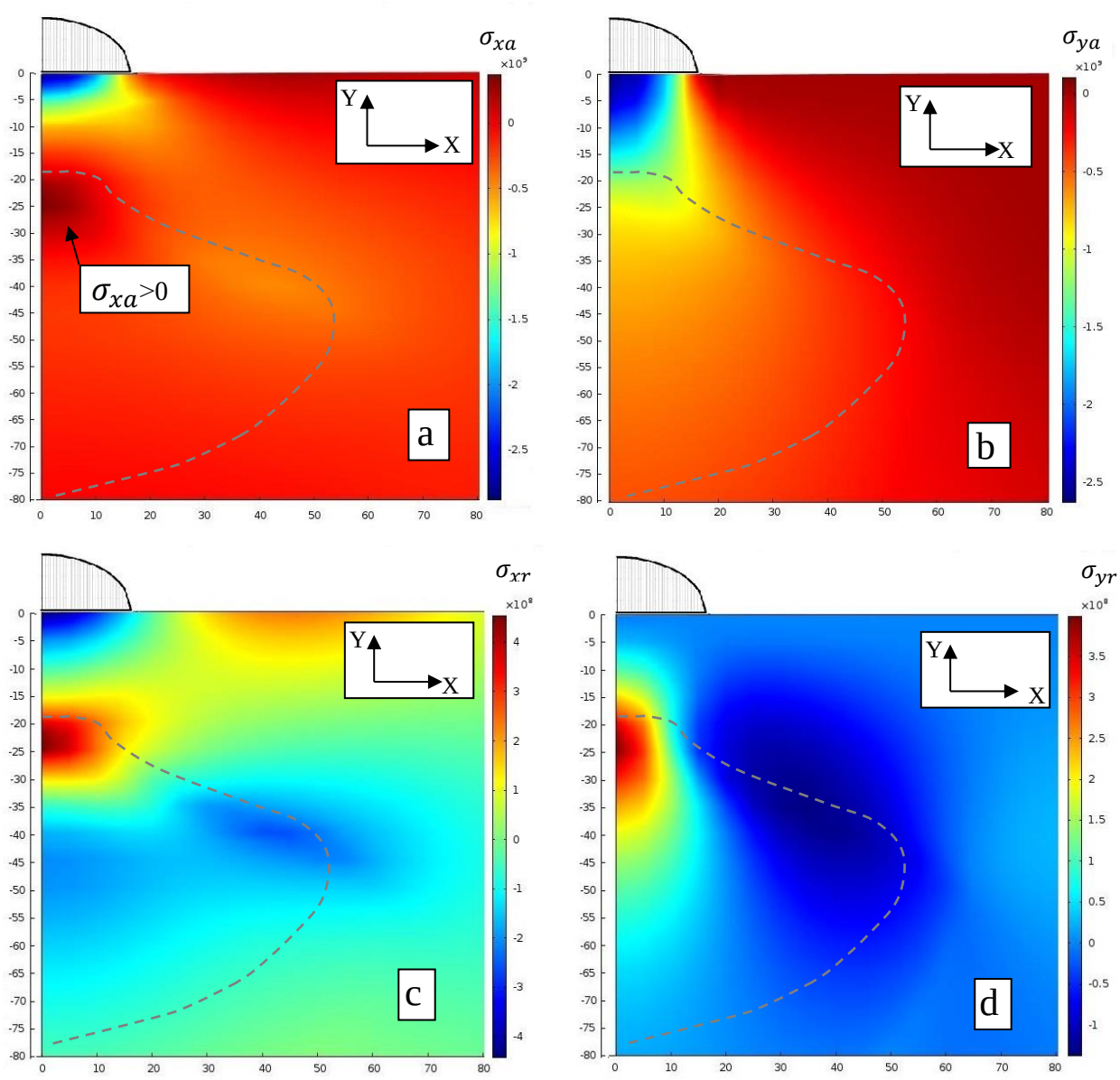

Figure 7. Distributions of the operational stresses (σ_{xa}, σ_{ya}) and the residual stresses (σ_{xr}, σ_{yr}) due to contact loading of case-hardened body with the depth of the hardened layer of 46 mm (as in Figure 3, curve 2). Contact length $2b = 35$ mm, contact load $F_n = 60$ kN/mm. Distribution of contact pressure is shown schematically to indicate the contact length. Coordinates X and Y are in mm, stress in N/mm^2. The dashed line indicate the boundaries of the plastic zone formed during loading.

After load removal the distributions of the residual stresses σ_{xr} and σ_{yr} exhibit an extremum. Both the stresses reach their maximum values on the axis of symmetry Y close to the upper boundary of the plastic zone and form regions of hydrostatic tension. Maximum values of the residual stresses are located at the depth of $17 - 35$ mm, which is about (1-2)b. Significant tensile residual stresses σ_{xr} develop at the free surface close to the preceding contact zone.

It also follows that with formation of the plastic zone, the operational stress σ_{xa} undergoes significant perturbation, while the distribution of σ_{ya} practically remains unchanged. Figure 8 shows the distributions of the operational stresses (σ_{xa} and σ_{ya}) and residual stresses (σ_{xr} and σ_{yr}) for different parameters of the 46 mm deep hardened surface layer. In the distribution of σ_{xa}, monotonously compressive in the elastic case (Figure 8a, curve 4), a zone of tensile stress forms with the inception of

plastic deformation (Figure 8a, curves 1,2). Their magnitude and depth depend on the parameters of the graded layer and loading conditions.

Analysis of the presented data shows that an increase in the core hardness, at the same depth of the hardened case, allows to significantly reduce both the operational and the residual tensile stresses in the graded layer. The location of the developed maximum stresses remains practically unchanged. An increase in the thickness of the hardened layer, with the same surface and core hardness, leads to a decrease of the operational and residual stresses in the graded layer, and increases the depth of the maximum tensile stresses.

Translation of the maximum residual stresses deeper into the thicker graded layer has a number of advantages. Firstly, due to further operation of the roll in the designed regime ($2b = 20$ mm, $F_n = 20$ kN/m) the cumulative stresses at the depths of 5-15 mm, where the maximum effective stresses act, is transferred into the compressive zone, more favorable for the material behavior under variable stress

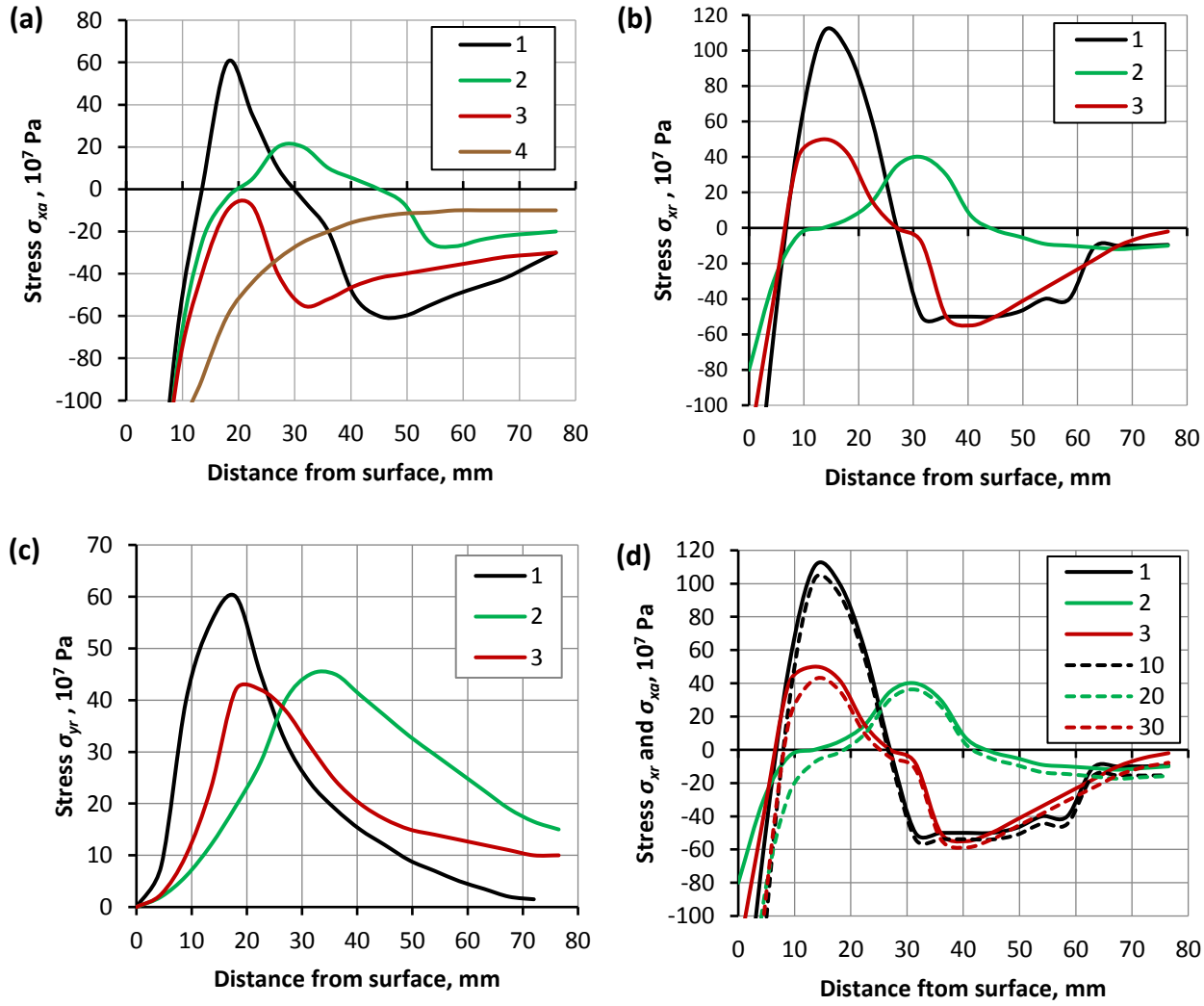

Figure 8. Distribution of the operational stress σ_{xa} and the residual σ_{xr}, σ_{yr} along the axis of symmetry Y for different parameters of the hardened surface layer for the contact length $2b = 35$ mm and contact load $F_n = 100$ kN/mm: a) Distribution of the operational stress σ_{xa}; b) σ_{xr}; c) σ_{yr}; d) distribution of the residual stress σ_{xr} and the cumulative operational stress during subsequent loading with standard designed load. Curve legend: 1 - total depth of the hardened layer $H_z = 46$ mm, softer core; 2 – $H_z = 72$ mm, softer core; 3 - $H_z = 46$ mm, harder core; 4 – though-hardened material; 10,20,30 – cumulative operational stress at reloading with nominal/designed load for the parameters of the graded layer described by 1,2,3, respectively.

(Figure 8d, compare curves 1 and 10 versus 2 and 20, respectively). Secondly, the range of changes of the cumulative stresses is significantly lower.

Figures 9 and 10 show the maximum values of the operational σ_{xa} and residual σ_{xr} stresses and their location in the graded surface layer as functions of the total contact force at overload. Figure 9 shows the maximum operational and residual stresses, σ_{xa} and σ_{xr}, respectively, in the subsurface depths of $10 - 60$ mm for different loading conditions on the contact zone length of $2b = 35$ mm and 65 mm.

With development of a plastic zone, the magnitudes of the maximum operational and residual stresses depend both on the contact stresses and on total contact forces in the contact zone, as well as the parameters of the graded layer (Figure 9). After the load removal, the values of the residual tensile stresses are significantly higher than the operational stresses at the same applied load (compare lines in Figure 9a and 9b, and Figure 9c and 9d). Nevertheless, no secondary plastic zone has been observes in

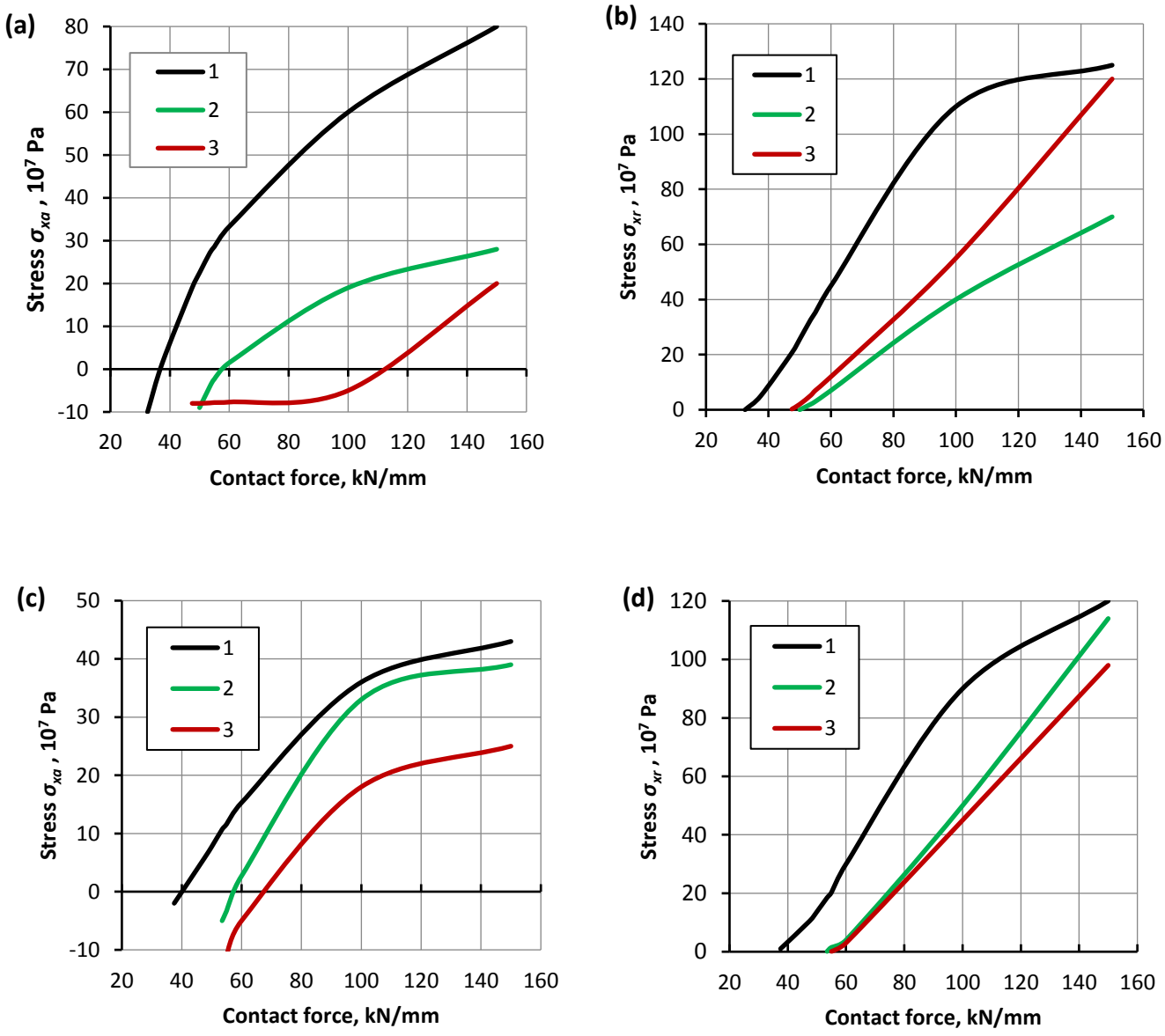

Figure 9. Maximum values of the operational σ_{xa} (a),(c) and residual σ_{xr} (b),(d) in the near-surface depths of 10-60 mm for different parameters of the hardened layer. (a) and (b) - contact length $2b = 35$ mm; (c) and (d) – contact length $2b = 65$ mm. Curve legend: 1 – total depth of the hardened layer $H_z = 46$ mm, softer core; 2 - $H_z = 72$ mm, softer core; 3 - $H_z = 46$ mm, harder core.

the unloaded material. This is explained by the fact that the tensile residual stress field has a very large hydrostatic (spherical) component, while the deviatoric part is small.

Figure 10 shows the location of the maximum values of the operational σ_{xa} and residual σ_{xr} for different parameters of the graded layer and loading conditions. It can be observed that the increasing contact load moves the depth of the maximum operational and residual stresses closer to the surface, while the location of the maximum residual stresses are closer to the surface than the corresponding maximum operational stresses.

Analysis of the residual stresses in the graded half-plane after unloading indicates that the previously formed plastic zone results in formation of a residual stress field with marked hydrostatic (spherical) tensile component. Figure 11 shows the distributions of the residual hydrostatic stress σ_{hr} along the axis of symmetry Y for different parameters of the graded layer with the contact zone of $2b = 35$ mm and the contact force $F_n = 100$ kN/mm. The distributions are very close to the ones for σ_{xr}.

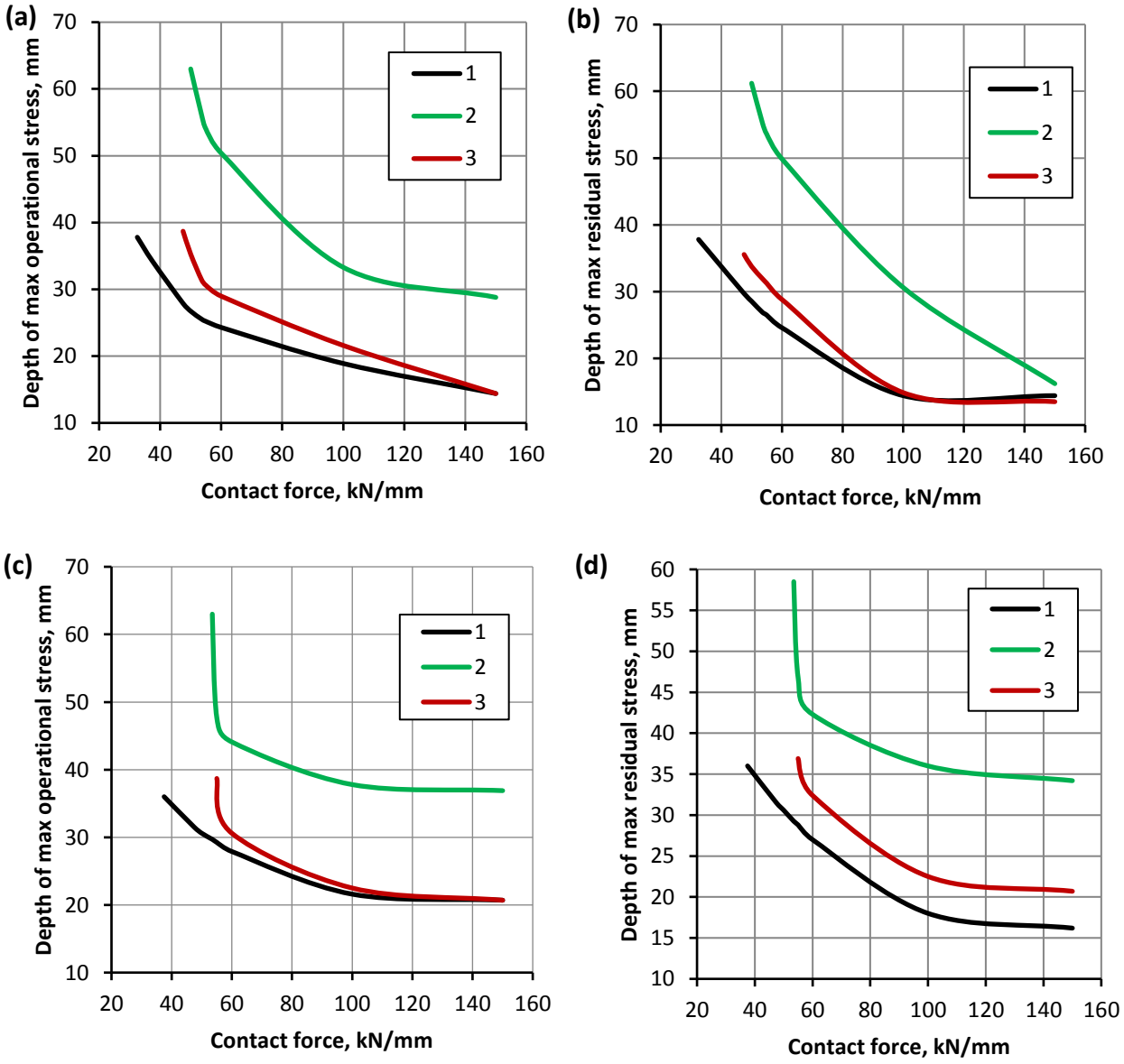

Figure 10. Depth of maximum operational stress σ_{xa} (a),(c) and the residual σ_{xr} (b),(d) as a function of the contact force F_n in the near-surface layer. (a) and (b) - contact length of $2b = 35$ mm; (c) and (d) - $2b = 65$ mm. Curve legend: 1 – total length of the hardened layer $H_z = 46$ mm, softer core; 2 - $H_z = 72$ mm, softer core; 3 - $H_z = 46$ mm, harder core.

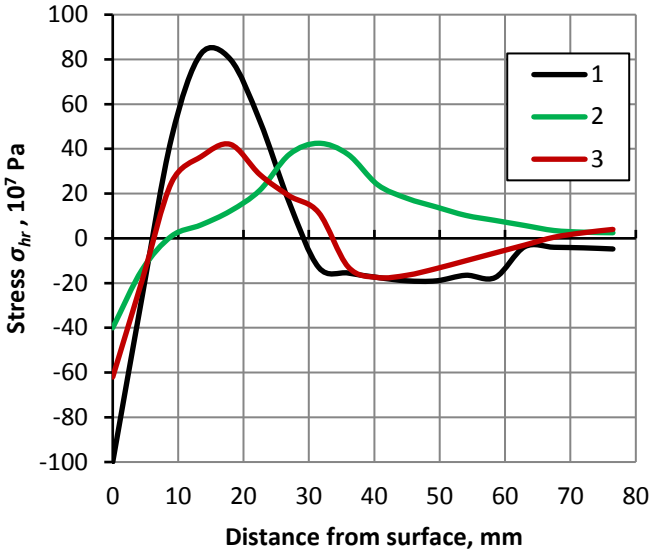

Figure 11. Distribution of the hydrostatic residual stresses (σ_{hr}) along the axis of symmetry Y. 1 – total depth of the hardened layer $H_z = 46$ mm, softer core; 2 - $H_z = 72$ mm, softer core; 3 - $H_z = 46$ mm, harder core.

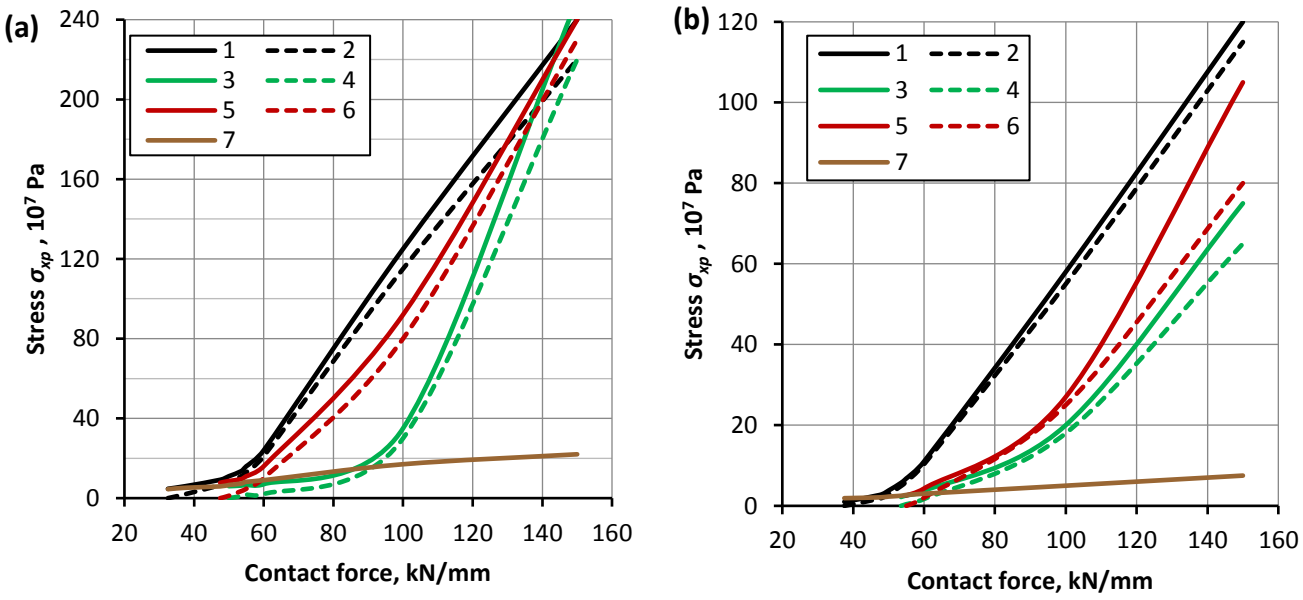

Figure 12. Maximum tensile operational stresses (curves 1,3,5,7) and maximum tensile residual stresses (curves 2,4,6) at the free surface in the vicinity of the contact zone. (a) – contact length $2b = 35$ mm; (b) - $2b = 65$ mm. Curve legend: 1,2 – total thickness of the hardened layer $H_z = 46$ mm, softer core; 3,4 – $H_z = 72$ mm, softer core; 5,6 – $H_z = 46$ mm, harder core; 7 – through-hardened elastic material.

High tensile stresses, both operational and residual, are also observed at the surface in vicinity of the contact zone. Figure 12 shows the dependence of the maximum operational and residual tensile stresses at the surface of the graded half-plane for the cases $2b = 35$ mm and (Figure 12a) and $2b = 65$ mm (Figure 12b). Maximum surface stresses in the perfectly elastic half-plane are also presented in Figure 12 (curve 7). It can be observed that formation of a plastic zone in the graded layer yields an increase in the surface stresses in up to 10 times. Shorter contact length (higher mean contact stress), all other factors being the same, leads to a proportional increase in the surface stress magnitudes.

5. Summary

The near-contact zone experiences high level of stresses, especially with short contact lengths and high contact loads. The most critical zone is the top boundary of the plastic zone. Here the hardened material is subjected to tensile stresses during overloading, and then the cumulative effect of stress field during further operation of the roll is characterized by a significant tensile spherical part of the residual stress field. Maximum tensile stresses develop at the boundary between the elastic and plastic zones; as well, tensile stresses develop at the free surface in the vicinity of the contact zone. Hardened steel with low plastic capacity is very sensitive to tensile stresses, which can lead to premature crack formation and failure. Following an overloading, operation of the overloaded roll induces non-symmetric cyclic loading, where the operational stresses superimpose on the tensile residual stresses that form the main part of the mean cycle stress.

Experiments show that with the mean stress of 0.4 GPa, the endurance limit of steel reduces by the factor of 2, while for 0.8 GPa – 6 times and more. Therefore, in our basis realization of the hardened case, significant decrease in the endurance limit of the material is expected at depths 10-20 mm, where the maximum tensile stresses have magnitudes of 0.8-1 GPa; hence, a higher probability of spalling is expected at these depths. It is interesting to note, that in engineering practice local spalling and delamination in cold rolling mill rolls are often observed at the depth of 10-20 mm [1,4-6].

Increasing the hardness of the roll core material allows to reduce the maximum tensile stresses in the critical locations more than twice. Increasing the thickness of the hardened case leads to zero and even negative residual stresses within the critical layers. According to experimental data [2], compressive mean cycle stresses of -0.4 GPa and -0.8 Gpa increase the endurance limit of a quenched steel in up to 1.5 times and 2 times, respectively. Therefore, thicker hardened case would improve resistance of cold rolling mill rolls to local overloads. It is important to note that the analysis presented herein is also valid in the case of normal operation of rolls with insufficient depth of the hardened case (see e.g. [17-19]), either due to technological/manufacturing error or unsuitable design.

It should be noted that the presented results have been obtained for a frictionless normal contact between an elastic cylinder and a plastically graded (surface-hardened) half plane. The suggested methodology is applicable for analysis of the effects of local overloads on durability and serviceability of any surface-hardened mechanical parts. Some parameters of realistic contact conditions during an overload of cold rolling mill work rolls, such as contact friction, rolling speed, specific distribution of contact stresses along the contact, curvature of the surfaces in contact, dynamical response of the roll to an overload, etc., remained beyond the scope of the presented analysis, although can have significant effects on formation of sub-surface plastic zones in the rolls. These effects should be carefully investigated for a deeper understanding of the underlying deformation processes, and for developing accurate design methodologies for case-hardening of the rolls in view of potential overloads.

Bibliography

1. Roberts, W.L., *Cold rolling of steel*. 1978, New York: M. Dekker.
2. Serensen, S.V., V.P. Kogaev, and R.M. Shneiderovich, *Bearing capacity and strength calculation of machine parts: Handbook*. 1975: Mashinostroenie, Moscow. (in Russian)
3. Johnson, K.L., *Contact mechanics*. 1987, Cambridge University Press, Cambeidge.
4. Bolt, P.H., et al., *Damage resistance and roughness retention of work rolls in cold rolling mills.* Revue de Métallurgie, 2010. 107(6): p. 245-255.

5. Bolt, P.H., et al., *Damage resistance and roughness retention of work rolls for cold rolling and temper rolling (toprolls).* Final report. 2013. DOI: 10.2777/95330.
6. Ray, A.K., et al., *Life of rolls in a cold rolling mill in a steel plant-operation versus manufacture*. Engineering Failure Analysis, 2000. 7(1): p. 55-67.
7. Tsun, A.M., *Modelling of local overloadings of rolls in thin sheet rolling*. 1985, Magnitogorsk Technical University. Magnitogorsk
8. Polukhin, V.P., Nikolaev, V.A., Tylkin, M.A, et al., *Reliability and durability of cold rolling rolls*, Metallurgiya, Moscow (1976), (in Russian)
9. Devyatchenko, L.D., Tsun, A.M. and Tikhonovsky, M.G., *Statistical analysis of operating conditions of work rolls during cold rolling*. Steel USSR, 1982 **12**(11).
10. Wusatowski, Z., Fundamentals of Rolling. 1969, Pergamon Press
11. Tselikov, A.I., Grishkov, A.I. *The theory of rolling*, Metallurgiya, Moscow, 1970, (in Russian).
12. Ginzburg, V.B. and Ballas, R., *Flat rolling fundamentals*. 2000, New York: Marcel Dekker.
13. Stone, M.D., *The rolling of thin strip - Part I*. Iron and Steel Engineer Year Book, 1953, p. 115-128.
14. Tong, K. and Sachs, G., *Roll-separating force and minimum thickness of cold-rolled strips.* Journal of the Mechanics and Physics of Solids, 1957. **6**(1): p. 35-46.
15. Vinogradov, V., Knyazhansky, M., and Tsun, A. *Experimental observation and numerical modeling of formation of local plastic zones in hardened surface layers due to contact overloading.* Mechanics of Materials, 2015. 83: p. 90-102.
16. Comsol Multiphysics, Reference Guide, http://www.comsol.com
17. Azevedo, C.R.F. and J.B. Neto, *Failure analysis of forged and induction hardened steel cold work rolls.* Engineering Failure Analysis, 2004. **11**(6): p. 951-966.
18. Li, H.C., Jiang, Z.Y., Tieu, K.A., Sun, W.H., *Analysis of premature failure of work rolls in a cold strip plant*. Wear, 2007. **263**: p.1442-1446.
19. Ghosh, S., Sinha, P., Indimath, S. et al. *Ribbon fatigue spalling of a forged work roll used at a cold rolling mill*, J Fail. Anal. and Preven. 2014, 14, pp:707-714. DOI:10.1007/s11668-014-9885-4